10TH INTERNATIONAL SYMPOSIUM ON PARTICLE IMAGE VELOCIMETRY – PIV13
Delft, The Netherlands, July 1-3, 2013

Three-dimensional wake reconstruction of a flapping-wing MAV using a Kriging regression technique

M. Percin[1], J.H.S. de Baar[1], B.W. van Oudheusden[1], R.P. Dwight[1]

[1]Faculty of Aerospace Engineering, Delft University of Technology, Delft, The Netherlands
m.percin@tudelft.nl

ABSTRACT

The work explores the three-dimensional unsteady wake of a flapping-wing Micro Air Vehicle (MAV) 'DelFly II', applying a Kriging regression technique for the spatial regression of time-resolved Stereoscopic Particle Image Velocimetry (Stereo-PIV) data. In the view of limited number of measurement planes, the particular objective of the regression is to provide an accurate volumetric representation of the measurement domain on a spatial grid that is much finer than the spacing between the measurement planes. A unique feature of the current study is the incorporation of a statistical error model in the Kriging regression process as an estimate of the local measurement uncertainty of the PIV measurements. The performance of the Kriging regression technique with local error estimates is evaluated based on direct comparisons to measurement data. As a final result of the regression, three-dimensional vortical structures are reconstructed and it is shown that each of two wings generates separate vortex loops and sheds two trailing edge vortices during the downstroke phase. On the other hand, the structures of upper and lower wings occasionally interact with each other during the upstroke phase. Wake structure displays major differences in terms of vortex formations for different reduced frequencies.

INTRODUCTION

Flapping wing flight has attracted increased interest among aerodynamics researchers recently in view of the expansion of design efforts in the field of Micro Aerial Vehicles (MAVs) [1]. MAVs are receiving specific attention because of their potential as mobile platforms capable of reconnaissance and gathering intelligence in hazardous and physically inaccessible areas. To achieve these missions, the MAV should be maneuvering with ease, while staying aloft and propelling itself efficiently. Conventional means of aerodynamic force generation are found lacking at this point and the flapping-wing approach, which has been improved in millions of years of evolution in nature, becomes an appealing or even necessary alternative solution. In contrast to the conventional (fixed and rotary wing) force generation mechanisms, flapping wing systems take benefit from the unsteady flow effects that are associated to the vortices separating from the wing leading and trailing edges, which create low pressure regions around the wings that lead to the generation of higher lift and thrust.

DelFly II [2], which is the subject of investigation for the current paper, is a bio-inspired flapping wing MAV designed and built at Delft University of Technology. The DelFly has a bi-plane wing configuration (Figure 1) with wings which consist of Mylar foil, reinforced with carbon rods. It has a total wing span of 280 mm, and weighs 17 g. A custom made brushless motor with a motor controller, a gear system and a crank shaft mechanism are used to drive the wings in flapping motion. A conventional cross-tail is used in order to guarantee stability and controllability. The DelFly can hover as well as fly in forward and backward direction. An essential part of the DelFly MAV system is that it is equipped with a miniature onboard camera, not only for observational purposes but also for making autonomous flight possible by use of the image analysis software in the ground station.

The DelFly flapping biplane wing configuration displays the so-called clap-and-fling phenomena, as a means of additional thrust and lift production. This effect was first described by Weis-Fogh [3] as a novel lift enhancement mechanism observed in animal flight and which is based on wing-wing interaction that takes place at the wing stroke reversal. During this phase in the flapping cycle, the leading edges of the wings come together and they pronate about their leading edges until the gap between them is closed in the clap phase. The fling phase starts with supination about the trailing edges and continues with the outward translation of the wings. Experiments on insects revealed that use of clap-and-fling motion increases aerodynamic lift per unit flight muscle by 25% with respect to conventional flapping motions [4]. Furthermore, the flexibility of the wings was shown to be an important parameter for the clap-and-fling motion. With the effect of flexibility, the wings tend to stick together with the fling occurring more like a peel and clap more like a reverse peel [5]. From aerodynamic loading point of view, it was shown that flexibility increases lift and decreases drag [6]. Aerodynamics of the clap-and-fling motion of the DelFly wings has been investigated in a number of previous experimental studies. De Clercq [7] performed Stereo-PIV experiments in the vicinity of the flapping wings

of the DelFly in hover condition with simultaneous thrust (viz. lift) measurements. She described the clap-and-peel type flapping motion of the DelFly wings and found that the LEV at the onset of the fling phase increases lift. Bruggeman [8] performed a wing optimization study which resulted in a 10% increase in thrust-to-drag ratio. Groen [9] compared the flow fields around the original and improved DelFly wings and described the different behavior of LEVs, linking them to changes in flexibility behavior.

Figure 1 DelFly in flight

Notwithstanding that the measurements in the vicinity of the flapping wings of the DelFly have provided substantial insight in the aerodynamic and aeroelastic behavior of the DelFly wings, the wake structure still remains largely unresolved. Also, all previous flow measurements were performed on the DelFly in a quiescent ambient environment, thus simulating the hovering flight mode. Therefore, the present investigation directs its attention to the wake formation behind the DelFly in the forward flight regime, simulated by placing the DelFly in the wind tunnel. The wake structure behind the flapping wings of the DelFly bears resemblance to the wake of flapping animal species. Extensive measurements have been performed in the wake of flapping wings of bats at the University of Lund, which have revealed the existence of closed-loop vortical structures during the flapping motion [10]. Muijres et al. [11] identified the aerodynamic features present in the wake of a *G. soricina* bat: the starting vortex, the tip vortex, the root vortex and a reversed vortex dipole (the latter structure may be formed during part of the upstroke when the wing is producing negative lift). They described formation of vortex loops as a result of interactions between these vortex structures during the flapping cycle.

It is clear that the wake structure of the flapping wings requires a detailed investigation, particularly for the DelFly case which has two wing pairs and a tail that is presumably interacting with the wake structures of the wings. Moreover, the complex unsteady characteristics of the related aerodynamics phenomena necessitate reconstruction of the three-dimensional wake structure of the flapping wings for the sake of thorough analysis. Therefore, time-resolved Stereoscopic Particle Image Velocimetry (Stereo-PIV) measurement were performed in the wake of flapping wings of the DelFly II in chordwise planes at a number of streamwise positions [12]. Then, Kriging regression technique [13] is used to reconstruct the three-dimensional wake of the flapping wings. In view of the limited number of measurement planes, the particular objective of the regression is to provide an accurate volumetric representation of the measurement domain on a spatial grid that is much finer than the spacing between the measurement planes. Whereas the use of Kriging regression for PIV data has been addressed in previous studies [14, 15], the unique feature of the present investigation is that a model of the local error of the PIV data is incorporated in the regression technique. This approach allows for a more reliable reconstruction of the wake topology than more conventional interpolation or regression procedures. A simplified PIV-error model is used, derived from the local correlation map for each vector in the current study. Furthermore, the Kriging regression technique is also used in order to calculate the spatial derivatives directly from the reconstructed flow, which are crucial for the visualization of vortical structures.

EXPERIMENTAL SETUP & DATA PROCESSING

The experiments were performed in one of the low speed wind tunnels at the Aerodynamic Laboratory of Delft University of Technology (TUDelft). The wind tunnel has an open test section with cross-section dimensions of 600 mm x 600 mm. The measurements were performed for free-stream velocities (U_∞) in the range of 2-6 m/s. The Reynolds numbers (Re) based on the mean wing chord-length (c) and free-stream velocity are in the range of 10,000-30,000. A complete DelFly II model was positioned in the test section of the wind tunnel in forward flight configuration, attached to a force balance mechanism. Experiments were conducted at four different angles of attack (α) of 0˚, 5˚, 10˚, and 15˚. In addition to the free-stream velocity and the angle of attack, also the flapping frequency (f) of

the DelFly wings was varied in the range of 6-12 Hz by use of a microcontroller system that was also utilized for the phase determination of the wings and synchronization of the PIV image acquisition.

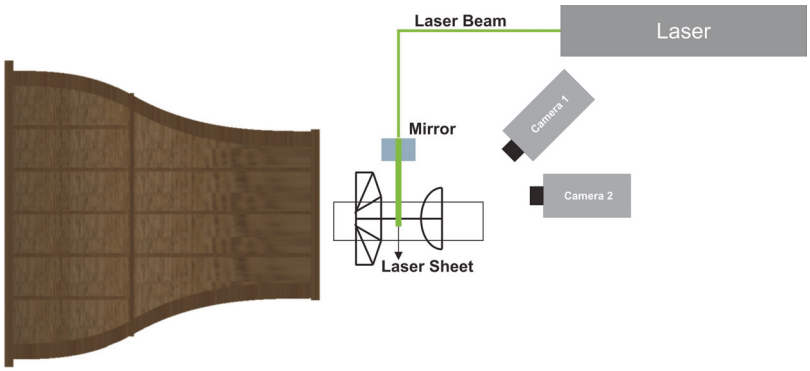

Figure 2 Sketch of the experimental setup in top view

High-speed stereo-PIV measurements were carried out in order to capture time-resolved three-component spanwise oriented planar velocity fields in the wake of flapping wings of the DelFly model. The flow was illuminated with a double pulse Nd:YLF laser (Quantronix Darwin Duo) with a wavelength of 527 nm. The laser sheet with a thickness of 4 mm was kept at a fixed position and the complete model and balance mechanism was shifted in order to perform the measurements in planes at different streamwise positions relative to the model. Measurements were thus performed at 12 consecutive planes with a distance of 10 mm in between each other (Figure 2). The first measurement plane was placed 10 mm downstream from the trailing edge of the wings. Water-glycol based fog of droplets with a mean diameter of 1μm, generated by a SAFEX fog generator, was employed as seeding for the PIV measurements. In order to achieve a homogenous seeding of the flow, the complete measurement room was filled with the fog beforehand. Images of the tracer particles were captured with three CMOS cameras (HighSpeedStar 6) with have a maximum resolution of 1024x1024 pixels at 5.4 kHz frame rate. The pixel pitch of the camera sensor is 20 μm. Each camera was equipped with a Nikon 60 mm focal objective and Scheimpflug adapter. It should be noted that the first two cameras (operated with numerical aperture of 4), which were placed above the test section with an angle of 40˚ with respect to each other, were primarily used for the stereo-PIV measurements. The third camera (with numerical aperture 2.8), which was placed at the same horizontal plane with the DelFly model, was utilized only when the tail caused considerable blockage in the view of the second camera. In that case, the first and the third cameras were employed for image acquisition, which were also positioned at an angle of 40˚ with respect to each other.

For each measurement plane a field of view of 200 mm x 200 mm was captured with a magnification factor of approximately 0.1 at a digital resolution of 5 pixels/mm. Double-frame image sequences of tracer particles were recorded with an acquisition frequency of 250 Hz. The time separation between two frames was 200 μs. Davis 8.0 (LaVision) was used in data acquisition, image pre-processing, stereoscopic correlation of the images, and further vector post-processing. The pre-processed double frame images were interrogated using windows of final size 64 pixels x 64 pixels with an overlap factor of 75% resulting in vector spacing of 3 mm in each direction. Special care was taken to phase-synchronize the data for the different planes, to allow a reconstruction of the three-dimensional wake structures throughout the flap cycle. Under the present conditions, the non-constant reflections from the flapping wings posed a particular complicating factor for the PIV measurement, resulting in significant variations in imaging conditions, which formed a major motivation for using the Kriging regression approach.

KRIGING REGRESSION WITH A LOCAL ERROR ESTIMATE

The three-component planar velocity fields, together with local Peak-to-Peak Ratio (PPR) values, are utilized in the Kriging regression process to reconstruct the wake topology. In the following we will present Kriging in a Bayesian framework, which: 1) enables a solid definition of the Kriging machinery and 2) invites a clear interpretation of that same machinery in the context of fluid dynamics.

The Bayesian framework deals with probability distributions. Some general ingredients of a Bayesian analysis are the *Quantity of Interest* (QoI), *prior*, *data*, Bayes' Rule, and *posterior*. We start with a prior for the QoI, which is basically a rough but informed guess. The acquisition of the data is part of an experiment and is considered to be subject to measurement uncertainty. Through Bayes Rule, we use the data to update the prior, after which we arrive at a posterior for the QoI. As such the posterior predicts the QoI *conditional* on the data, and the mean of this posterior serves as an estimate of the QoI.

Kriging was developed independently in the field of Geology [16] and of Meteorology [17], and nowadays is a well-known method for optimal spatial regression [18, 19]. Kriging can be formulated in a Bayesian framework [20], which increases clarity of definition, flexibility, and ease of interpretation. In PIV post-processing, the context of fluid dynamics invites some nice interpretations that we would like to include in the following discussion.

We consider a set of measurements Y of the Quantity of Interest X:

$$Y = HX + N(0, \varepsilon) \tag{1}$$

In the present context, X represents the flow velocity field and Y the PIV data. The Gaussian measurement uncertainty $N(0,\varepsilon)$ is assumed to be unbiased and of magnitude ε. Note that from Equation (1) the PIV data Y is generally different from the flow field X due to discrete sampling and measurement error, an interpretation which corresponds well with the limitations of a PIV experiment. The objective of Kriging regression is to optimally reconstruct the flow field X given the PIV data Y.

The Kriging estimator for the flow field X conditional on the data Y can be derived from Bayes' Rule, this derivation results in [20]:

$$E(X|Y) = \mu + PH^T(R + HPH^T)^{-1}(Y - H\mu) \tag{2}$$

Equation (2) is contains several terms, the building blocks of the 'Kriging machinery'. First of all, the quantity μ is the (mean of the) prior for the flow velocity. The Kriging predictor Equation (2) will use the PIV data to update this prior flow field and arrive at the posterior. A rough but informed guess of μ can be given by the free-stream flow velocity, or – when sufficient data is available – it is acceptable to use the statistical mean of the data instead.

As we have seen in Equation (1), the observation matrix H selects the measurements from the flow field. In fluid dynamics we might consider velocity values for X on a high-resolution grid, and observations Y on a much coarser grid. The observation matrix H is a rectangular matrix with ones and zeros that selects the grid points for the coarse grid from the high-resolution grid.

A typical building block of the Kriging machinery is the covariance matrix P, which is constructed from a 3-dimensional correlation function. In fluid dynamics, the correlation function invites the following interpretation: For a hypothetical flow field X we could make a cross-correlation map. This cross-correlation map would have a maximum of one in the center, and would decrease when we move away from the center. What we see in this map is that velocity vectors that are close to each other can be highly correlated, while velocity vectors that are separated by a longer distance are hardly correlated. The width of the central peak in the cross-correlation map is quite valuable information if we want to reconstruct the flow field from PIV data, as it indicates how fast velocity vectors become uncorrelated when we increase their distance – evidently this would characterize the size of important structures in the flow. Although we are considering a hypothetical flow field and presently the exact 3-dimensional correlation map is not at our disposal, we can – again in the case of sufficient data – use a simple parameterized correlation function that summarizes the main characteristics we would expect to find in the correlation map: This parameterized correlation function constitutes the prior correlation matrix P. The choice of Gaussian correlation functions has been found to perform well for similar flows [14] and at the same time enables the computation of smooth derivatives of the reconstructed flow.

For the Gaussian correlation function we will have to estimate three hyperparameters: the width of the Gaussian in each of the three spatial dimensions. Standard but expensive methods to determine these hyperparameters are a Maximum Likelihood Estimate (MLE) or a Sample Variogram (SV) [19]. However, such methods are unfeasible for large datasets like the present one. In order to limit the computational cost, a Frequency-domain Sample Variogram (FSV) method is used to estimate the correlation lengths [21]: A 3-dimensional Gaussian surface – the Fourier transform of the Gaussian correlation function – is fitted to the power spectrum of the data. The width of this surface is inversely related to the width of the correlation function: a smooth (oscillatory) flow field will have a spiky (flat) peak in the power spectrum.

The error matrix R is a covariance matrix which represents the measurement uncertainty, and has a central role in the present approach. Generally, this error matrix R is ignored when Kriging is used to post-process PIV data. However, this can lead to a sub-optimal reconstruction of the flow field, especially in the presence of a spatially dependent reliability of the PIV data. Presently, we assign a local measurement uncertainty ε_i to each individual PIV vector. Although we do not know the exact local measurement uncertainty, we propose to use a low-fidelity statistical model of the local measurement uncertainty. The PPR values, which can be regarded as a measure of the velocity vector reliability [22], are used as a proxy for the local measurement uncertainty in the low-fidelity uncertainty model:

$$\varepsilon_i \propto (\mathrm{PPR}_i - 1)^{-p} \quad (2)$$

For small data sets we can use cross-validation to optimize the model constant p, for larger data sets we use a deadlock method (with the underlying assumption that the reconstructed flow should be stationary with respect to the model constant). As long as the low fidelity uncertainty model captures the local fluctuations in measurement uncertainty, it is found to result in a more accurate reconstruction of the flow field. Although it is computationally more expensive to implement an estimation of the error for each measurement point, the benefits cannot be ignored as depending on the region of measurement, the reliability of PIV results can vary due to limitations of the experimental setup, such as severe reflections, shadows, and particle density.

RESULTS

In this section, first the performance of the wake reconstruction process by applying Kriging regression technique with local uncertainty estimate is tested by comparing the interpolated data to the measurement data. Then, preliminary results for the wake structure of the flapping DelFly wings are presented.

Performance of Kriging

We use three methods to determine the quality of the Kriging regression of the present flow field: 1) visual comparison of the 3-dimensional wake, 2) visual comparison of a single plane, and 3) quantitative validation of the 3-dimensional wake. A key point in these comparisons is that at first, out of 24 measurement planes only the 12 odd-numbered planes were available, due to synchronization issues with the remaining even-numbered planes. Therefore, initially all results were based on 12 measurement planes.

Visual comparison of the 3-dimensional wake

In order to test the success of Kriging regression technique, a particular data set which consists of 24 measurement planes with a distance of 5 mm between each other was used. Initially, the complete wake of the flapping wings was reconstructed by using 24 measurement planes. Kriging regression technique is utilized at this point to fill the gaps in measurement planes that originate from masked regions and are essentially the regions where mostly free-stream velocity is dominant and no prominent vortical structures are observed. On the other hand, the same wake is reconstructed again by using every other measurement plane (12 measurement planes) and Kriging regression technique to interpolate one plane in between measurement planes, which results in the same spatial resolution in the streamwise direction. Iso-surfaces of vorticity magnitude for both cases are plotted in Figure 3.

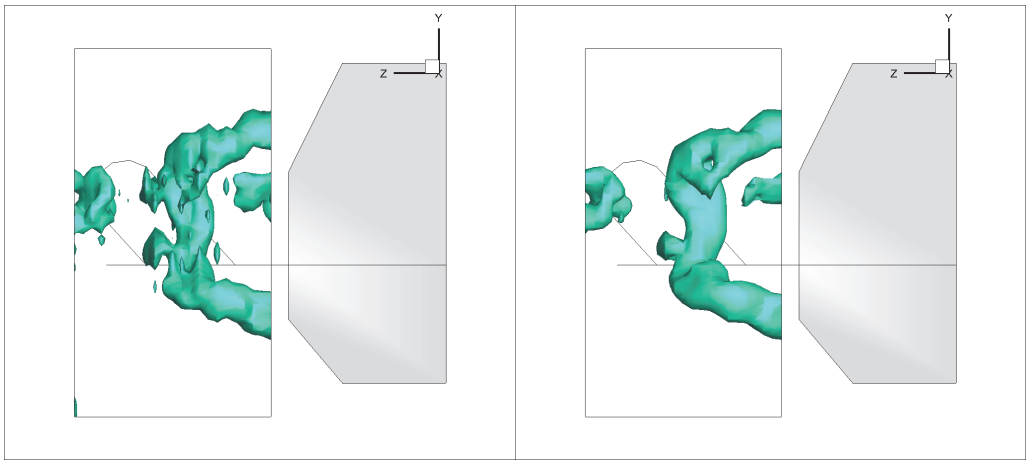

Figure 3 Iso-surfaces of vorticity magnitude (isovalue=0.125 s^{-1}) derived from two cases of wake reconstruction: Reconstruction of the wake from 24 measurement planes (left) and reconstruction of the wake by using every other plane and interpolating one plane in between by Kriging regression with local error estimates (right) (Side view of the wake of the DelFly)

It is clear that Kriging regression technique performs well in this case and apart from the small scale details, most prominent features of the vortical structures can be captured.

Visual comparison of a single plane

Using the data from the original 12 measurements planes, we reconstruct the flow field at the 11 intermediate planes. In Figure 4, we compare the reconstruction with the PIV data for one of the intermediate planes. The reconstructed flow field (on the right) corresponds well with the reference PIV data (on the left).

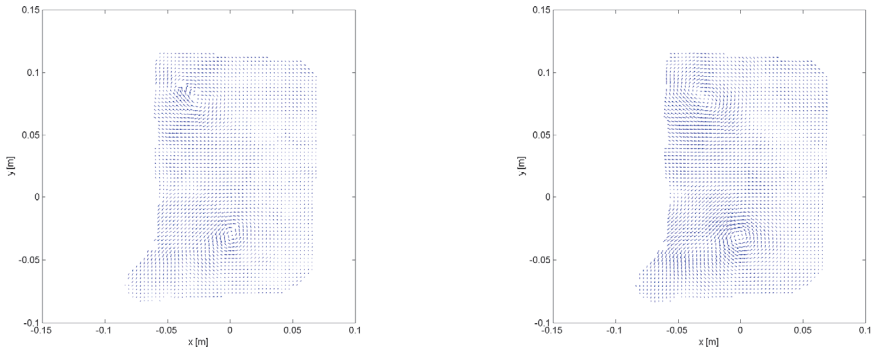

Figure 4 Comparison of the PIV data (left) and flow field reconstruction (right) for an intermediate measurement plane. Only 12 of the 24 available measurement planes were used as data during reconstruction, results are shown for a single intermediate plane

To visualize quantities such as vorticity and divergence, we will have to compute these quantities from the flow field. The straightforward approach is to use finite differencing to compute vorticity and divergence from the PIV data; however, this approach can be inaccurate due to grid spacing and measurement uncertainty. To mitigate this effect we apply 5×5 Gaussian smoothing to the PIV data before we compute vorticity and divergence, the results are shown on the left-hand side in Figure 5.

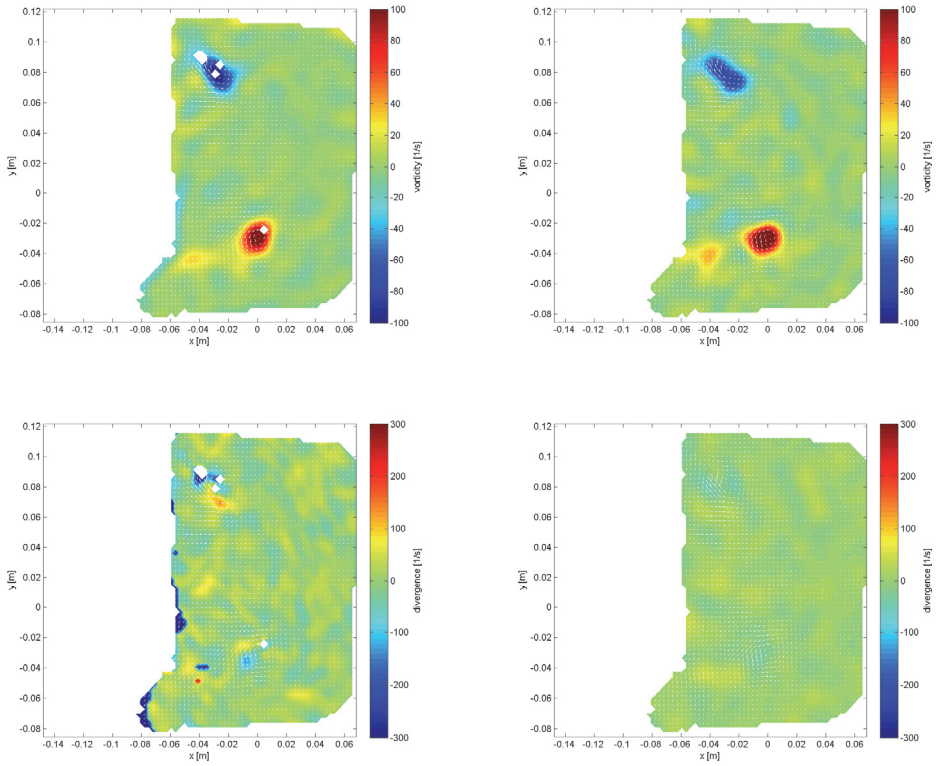

Figure 5 Comparison of the out-of-plane vorticity (top) and divergence (bottom) computed from smoothed PIV data (left) and from the reconstructed flow field (right). Only 12 of the 24 available measurement planes were used as data during reconstruction, results are shown for a single intermediate plane

After Kriging regression, we can compute the derivatives directly from the reconstructed flow field. The resulting vorticity and divergence are shown on the right-hand side in Figure 5. Clearly, the location, size, and magnitude of the reconstructed vortices (top right) agree well with those computed from the PIV data (top left). The divergence in the PIV data (bottom left) is quite significant, and shows some strong sources and sinks. As might be expected for a fairly incompressible flow, the divergence in the reconstructed flow field (bottom right) is much smaller and does not show strong sources or sinks.

Quantitative validation of the reconstructed wake

In Figure 4 and 5 we compared the results for a single intermediate measurement plane. To quantify the accuracy of the reconstruction, we use the PIV results of the intermediate plane as a reference and compute the Root Mean Squared Error (RMSE) of the reconstructed 3-dimensional wake.

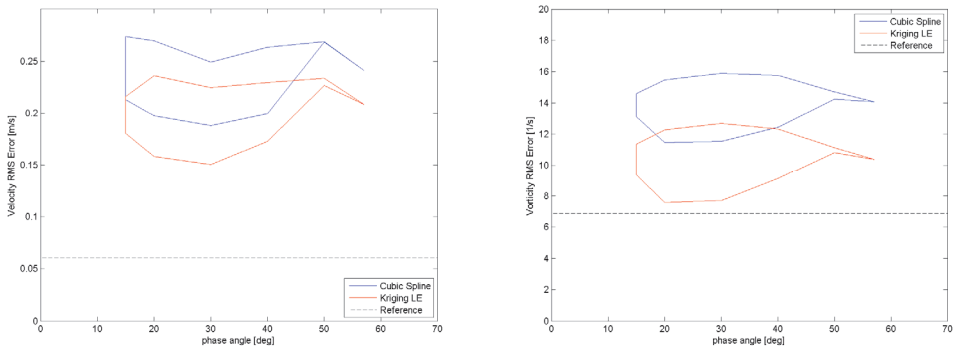

Figure 6 Cross-validation results for the velocity (left) and out-of-plane vorticity (right) of the reconstructed flow field. Only 12 of the 24 available measurement planes were used as data during reconstruction, the 11 intermediate planes were used as reference data

On the left in Figure 6 we see the cross validation results for the reconstructed velocity in the 3-dimensional wake. The RMSE is shown for cubic spline interpolation (blue) and Kriging regression (red). The dashed line is an indication of the noise level in the reference data. The RMSE depends on the phase of the flapping cycle, in general Kriging is more accurate than cubic spline interpolation. As might be expected, we see that the results for vorticity show a larger difference between cubic spline and Kriging interpolation. During part of the flapping cycle, the accuracy of the Kriging reconstruction is close to the noise level in the reference data.

It should be noted that application of the straightforward Kriging - without taking any (global or local) measurement uncertainty into account – results in highly inaccurate reconstruction of the flow field with RMSE of 6.7 m/s for the velocity and of 1.0×10^3 s^{-1} for the vorticity. These results are completely off-scale and have not been included in Figure 6.

Wake of the Flapping Wings

Notwithstanding that the experiments were performed for a wide range of experimental parameters, only the results for a selection of parameters at $Re = 15{,}000$ are discussed in this section. The three-dimensional wake of the flapping wings was reconstructed by use of Kriging regression technique with local uncertainty estimates based on PPR values. Two equi-distant planes were interpolated which results in a spatial resolution of 3.33 mm in the streamwise direction. Regarding to interpretation of the results, it should be noted that only one half of the wake is visualized (the wake is assumed to be nominally symmetrical) and that the region in the vicinity of the tail masked during PIV processing due to intensive reflection underneath and lack of illumination above the tail. Additionally, to assist the interpretation of the results, the DelFly wings are schematically displayed in the images as an indication of the flapping phase; however, they are represented as rigid bodies whereas in reality there is a significant amount of deformation on the wings during the flapping motion (Maximum trailing edge deformation with respect to rigid leading edge is 60% of the mean chord length [23]). Therefore, the position of vortical structures may occasionally seem to be uncorrelated with the position of the wings.

The general wake structures of the instroke and outstroke are shown for the case of $U_\infty = 3$ m/s, $f = 10$ Hz and $\alpha = 0^\circ$. The corresponding reduced frequency ($k = \pi f c / U_\infty$) is 0.84. In Figure 7, iso-surfaces of vorticity magnitude with an isovalue of 0.1 s^{-1} are shown for the non-dimensional time ($\tau = t \times f$) of 0.55, which corresponds to the end of

instroke, viz. clapping phase of the flapping cycle. In this phase, starting vortices of top and bottom wings (SV_t and SV_b), that are generated at the onset of the downstroke, are shed from the trailing edge and advected downstream. Additional trailing edge vortices are also shed into the wake during the downstroke (TEV_t and TEV_b). Prominent tip vortices of top and bottom wings (TV_t and TV_b) are present in the wake and these are connected to the trailing edge vortices. It is clear that there is no interaction between the upper and lower wing structures in the most part of the downstroke phase.

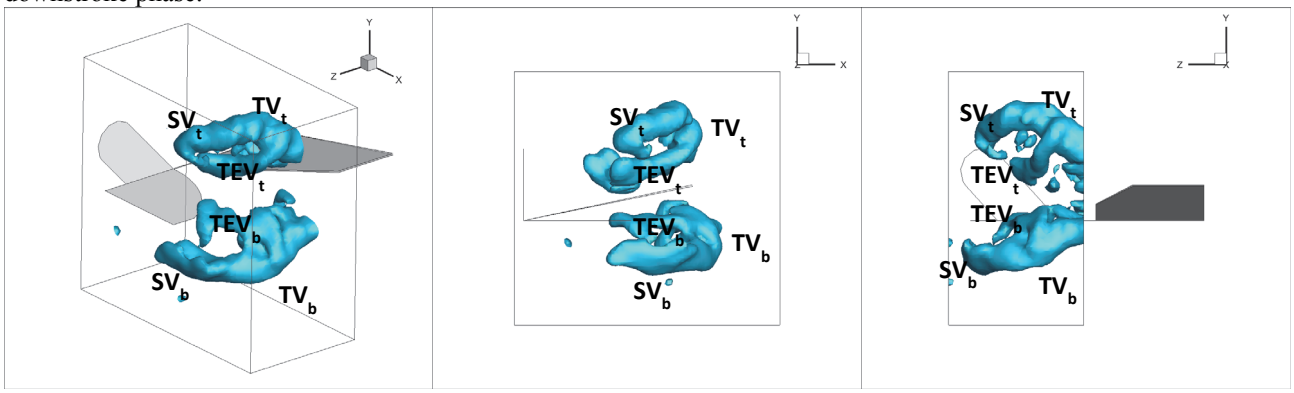

Figure 7 Iso-surfaces of vorticity magnitude (isovalue=0.1 s^{-1}) at the end of downstroke ($\boldsymbol{\tau = 0.55}$) – Perspective view (left), rear view (middle) and side view (right)

In Figure 8, vorticity magnitude iso-surfaces are plotted at $\tau = 0$, which is actually the start of the instroke. This particular moment is selected on purpose as the flow structures of the previous outstroke can be captured completely in the field of view (It should be noted that it takes time for the flow structures to appear in the field of view as the volume starts 10 mm downstream of the trailing edge). It is clear that, tip vortices of the top and bottom wings (TV_t and TV_b) forms a vortex loop which preserves its connection till the end of the upstroke. There is no sign of starting vortices or secondary trailing edge vorticity shed during the upstroke. It can be due to the diminished Wagner effect in the case of clap-and-fling motion [24] that results in weak trailing edge vorticity to be shed during the fling phase. However, it should be noted that these vortices might be in the vicinity of the tail and cannot be captured in the measurements due to improper illumination conditions in that region.

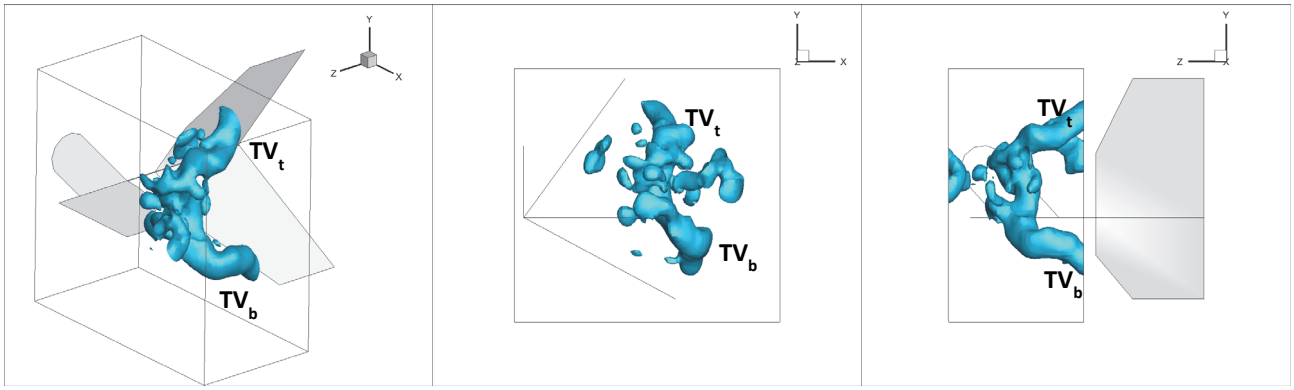

Figure 8 Iso-surfaces of vorticity magnitude (isovalue=0.1 s^{-1}) at the start of downstroke ($\boldsymbol{\tau = 0}$) – Perspective view (left), rear view (middle) and side view (right)

Wake structure at the end of the upstroke phase displays primary differences for the cases of different flapping frequencies (reduced frequencies) as shown in Figure 9. For the highest reduced frequency case, tip vortices of upstroke ($TV_{t,u}$ and $TV_{b,u}$) and previous downstroke ($TV_{t,d}$ and $TV_{b,d}$) are visible whereas for the lowest reduced frequency case, also root vortices of top and bottom wings are present in the wake (RV_t and RV_b). Apart from different vortical formations, the comparison suggests different formation and advection times for these vortical structures.

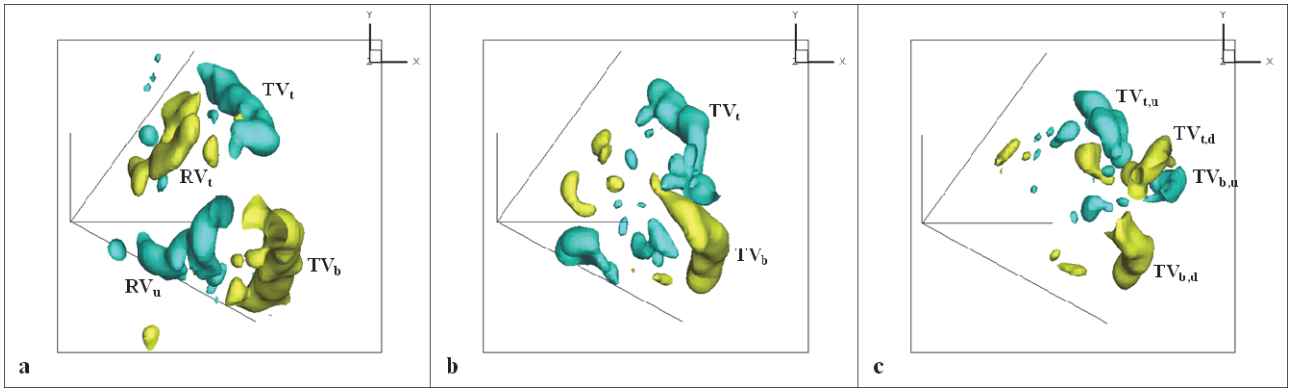

Figure 9 Iso-surfaces of z vorticity (rear view): a) $f = 6$ Hz, $U_\infty = 3$ m/s, and $\alpha = 0^\circ$ ($k = 0.5$) with isovalues of $\omega_z = \pm 0.03$, b) $f = 8$ Hz, $U_\infty = 3$ m/s, and $\alpha = 0^\circ$ ($k = 0.67$) with isovalues of $\omega_z = \pm 0.05$, c) $f = 10$ Hz, $U_\infty = 3$ m/s, and $\alpha = 0^\circ$ ($k = 0.84$) with isovalues of $\omega_z = \pm 0.03$

CONCLUSIONS

Three-dimensional wake of the flapping-wing MAV 'DelFly II' is studied experimentally via time-resolved Stereo-PIV technique. Three-component planar velocity fields were captured at different streamwise locations in the wake of the flapping wings. Then Kriging regression technique with local measurement uncertainty estimate was used for the reconstruction of the three-dimensional wake.

To evaluate the performance of the reconstruction technique, the flow field was reconstructed using three different methods: cubic spline interpolation, straightforward Kriging, and the present approach of Kriging with locally estimated measurement uncertainty. From visual comparison, the present approach gives the most accurate results. From quantitative validation, the present approach outperforms cubic spline interpolation as well as straightforward Kriging. In general, it can be concluded that – for noisy data – it is important to include an estimate of the measurement uncertainty (or noise level) in the Kriging analysis. This option is not available in standard Kriging software; however, a Matlab code that does include this option will soon be made available online at http://aerodynamics.lr.tudelft.nl/~bayesiancomputing/.

Wake structure of the flapping wings was reconstructed for a selection of parameters, i.e. flapping frequency, free-stream velocity and angle of attack. The general wake structure is described for the flapping cycle: shedding of starting vortex and secondary trailing edge vorticity during downstroke and vortex loop formed by the tip vortices of both wings during the upstroke. Comparison of cases of different flapping frequencies revealed different formations at the same time instants of the flapping motion suggesting different formation and advection time of vortical structures.

ACKNOWLEDGEMENTS

This research was supported by the Dutch Technology Foundation STW, grant number 11023 and 10113

REFERENCES

[1] Singh, B., and Chopra, I., "Insect-Based Hover-Capable Flapping Wings for Micro-Air Vehicles: Experiments and Analysis", AIAA Journal, Vol. 46, No. 9, 2008, pp. 2115-2135.
[2] de Croon, G.C.H.E., Groen, M.A., De Wagter, C., Remes, B.D.W., Ruijsink, R., and van Oudheusden, B.W.,"Design, Aerodynamics, and Autonomy of the DelFly," Bioinspiration and Biomimetics, Vol. 7, No. 2, 2012.
[3] Weis-Fogh, T., "Quick estimates of flight fitness in hovering animals, including novel mechanisms for lift production," The Journal Experimental Biology, Vol. 59, 1973, pp. 169-230.
[4] Marden, J., "Maximum lift production during take-off in flying animals," The Journal of Experimental Biology, Vol. 130, 1987, pp. 235–258.
[5] Ellington, C.P., "The aerodynamics of insect flight. IV. Aerodynamic mechanisms," Philosophical Transactions of the Royal Society B., Vol. 305, 1984, pp. 79–113.
[6] Miller, L.A., Peskin, C.S., "Flexible clap and fling in tiny insect flight," The Journal of Experimental Biology, Vol. 212, 2009, pp. 3076-3090.
[7] De Clercq, K.M.E., "Flow visualization and force measurements on a hovering flapping wing MAV DelFly II," M.Sc. thesis, Delft University of Technology, Delft, 2009.
[8] Bruggeman, B., "Improving flight performance of DelFly II in hover by improving wing design and driving mechanism," M.Sc. thesis, Delft University of Technology, Delft, 2010.

[9] Groen, M., "PIV and force measurements on the flapping-wing MAV DelFly II", M.Sc. thesis, Delft University of Technology, Delft, 2010.
[10] Hubel, T.Y., Hristov, N.I., Swartz, S.M., Breuer, K.S. "Time-resolved wake structure and kinematics of bat flight," Experiments in Fluids, Vol. 46, No.5, 2009, pp. 933-943.
[11] Muijres, F.T., Spedding, G.R., Winter, Y., Hedenström, A., "Actuator disk model and span efficiency of flapping flight in bats based on time-resolved PIV measurements," Experiments in Fluids, Vol. 51, No. 2, 2011, pp. 511-525.
[12] Eisma, J., "Flow visualization and force measurements on a flapping-wing MAV DelFly II in forward flight configuration", M.Sc. thesis, Delft University of Technology, Delft, 2012.
[13] Cressie N., "Statictics for spatial data," Wiley 1993.
[14] Venturi D. and Karniadakis G. E., "Gappy data and reconstruction procedures for flow past a cylinder," Journal of Fluid Mechanics, vol. 519, 2004, pp. 315–336.
[15] Gunes H. and Rist U., "Spatial resolution enhancement/smoothing of stereo particle-image velocimetry data using proper-orthogonal decomposition based and kriging interpolation methods," Physics of Fluids, vol. 19, 2007, 064101.
[16] Matheron, G., Principles of Geostatistics, Economic Geology, 58:1246–1266, 1963.
[17] Gandin, L., Objective analysis of meteorological fields: Gidrometeorologicheskoe Izdatel'stvo (GIMIZ), Leningrad, Translated by Israel Program for Scientific Translations, Jerusalem, 1965.
[18] Cressie, N., The origins of kriging, Mathematical Geology, 22(3):239–252, 1990.
[19] Cressie, N., Statistics for spatial data, Wiley, 1993.
[20] Wikle, C.K., Berliner, L.M., "A Bayesian tutorial for data assimilation," Physica D, Vol. 230, No. 1-2, 2007.
[21] J. de Baar, R. Dwight, and H. Bijl, Speeding up Kriging through fast estimation of the hyperparameters in the frequency-domain, Computers & Geosciences, Volume 54, April 2013, Pages 99-106
[22] Westerweel J., "Efficient detection of spurious vectors in particle image velocimetry data," Experiments in Fluids, Vol. 16, 1994, pp. 236-247.
[23] Percin, M., Hu, Y., van Oudheusden, B.W., Remes, B., Scarano, F., "Wing flexibility effects in clap-and-fling," International Journal of Micro Air Vehicles, Vol. 3, No. 4, 2011, pp. 217-227.
[24] Sane, S.P., "The aerodynamics of insect flight," The Journal of Experimental Biology, Vol. 206, 2003, pp. 4191-4208.